The tin sulfates $Sn(SO_4)_2$ and $Sn_2(SO_4)_3$: crystal structures, optical and thermal properties†

Matthias Hämmer, [a] Philip Netzsch, ‡[a] Steffen Klenner,[b] Kai Neuschulz,[c] Mona Struckmann,[c] Mathias S. Wickleder,[c] Michael Daub,[d] Harald Hillebrecht, [d] Rainer Pöttgen [b] and Henning A. Höppe *[a]

We report the crystal structures of two tin(IV) sulfate polymorphs **$Sn(SO_4)_2$-I** ($P2_1/c$ (no. 14), a = 504.34(3), b = 1065.43(6), c = 1065.47(6) pm, β = 91.991(2)°, 4617 independent reflections, 104 refined parameters, wR_2 = 0.096) and **$Sn(SO_4)_2$-II** ($P2_1/n$ (no. 14), a = 753.90(3), b = 802.39(3), c = 914.47(3) pm, β = 92.496 (2)°, 3970 independent reflections, 101 refined parameters, wR_2 = 0.033). Moreover, the first heterovalent tin sulfate **$Sn_2(SO_4)_3$** is reported which adopts space group $P\bar{1}$ (no. 2) (a = 483.78(9), b = 809.9(2), c = 1210.7(2) pm, α = 89.007(7)°, β = 86.381(7)°, γ = 73.344(7)°, 1602 independent reflections, 152 refined parameters, wR_2 = 0.059). Finally, **$SnSO_4$** – the only tin sulfate with known crystal structure – was revised and information complemented. The optical and thermal properties of all tin sulfates are investigated by FTIR, UV-vis, luminescence and ^{119}Sn Mössbauer spectroscopy as well as thermogravimetry and compared.

Introduction

Compounds comprising p block cations like Sn^{2+} are promising candidates for various applications like rare-earth free phosphors based on s–p transitions[1,2] or nonlinear optical (NLO) materials with large second-harmonic generation (SHG) effects due to stereochemically active lone pairs.[3–5] Recent examples for the latter are the first tin fluorooxoborate $Sn[B_2O_3F_2]$[6] or the first tin fluoride borate $Sn_3[B_3O_7]F$.[7] Moreover, sulfates show various interesting properties like ionic conductivity[8] and catalytic properties.[9] They also are suited as phosphor hosts and NLO materials due to their non π-conjugated tetrahedral SO_4^{2-} groups lacking inversion symmetry.[10,11] Consequently, the combination of both – tin cations and sulfate anions – might yield promising compounds. However, to date only three crystalline members are known for the ternary system Sn–S–O, *i.e.* $Sn_2(S_2O_4)_2$,[12] Sn_2OSO_4[13] and **$SnSO_4$**.[14,15] Despite the first report on the syntheses of tin sulfates or stannous sulfates in 1931[16] **$SnSO_4$** was to date the only pure tin sulfate with known crystal structure reported by Donaldson and Puxley in 1972.[14] It adopts a highly distorted variant of the *barite* structure comprising pyramidal SnO_3 units. Broadening the view, only three tin hydroxide oxide sulfates $Sn_3O(OH)_2SO_4$,[17] $Sn_6O_4(SO_4)(OH)_2$[18] and $Sn_7(OH)_{12}(SO_4)_2$[19] as well as the already mentioned oxide sulfate Sn_2OSO_4[13] have been reported. Notably, there are no reports on any homovalent Sn^{4+} compounds comprising sulfate groups without further cations like in $Ca_3Sn(SO_4)_2(OH)_6(H_2O)_3$[20] or $A_2[Sn(S_2O_7)_3]$ (A = Na, K, Ag, NH_4).[21] Although tetravalent tin sulfate $Sn(IV)(SO_4)_2$ had been mentioned multiple times,[22–25] no crystal structure was reported. Within their extensive study on the syntheses of various solid compounds prepared from Sn and H_2SO_4 Ahmed *et al.* proposed a polymorphism of $Sn(SO_4)_2$ and obtained unit cell parameters by indexing powder patterns for two polymorphs.[22] In general, all crystal structures of tetravalent metal sulfates $M(SO_4)_2$ (M = Ce, Zr, U, Th) known in literature adopt either the $Ce(SO_4)_2$ or the $Zr(SO_4)_2$ structure type.[26–28]

Apart from the mentioned heterovalent tin sulfate hydroxide $Sn(II)_6Sn(IV)(OH)_{12}(SO_4)_2$[19] Ahmed *et al.* reported the tin oxide sulfate $Sn(II)_2Sn(IV)_4O(SO_4)_9$ merely based on thermogravimetric data.[22] Further heterovalent oxidic tin compounds – crystallographically ordered in contrast to partially oxidised systems[29] – appear to be rare. Heterovalency is found in Sn

[a]*Institut für Physik, Universität Augsburg, Universitätsstraße 1, 86159 Augsburg, Germany. E-mail: henning@ak-hoeppe.de*
[b]*Institut für Anorganische und Analytische Chemie, Universität Münster, Corrensstraße 30, 48149 Münster, Germany*
[c]*Institute of Inorganic Chemistry, University of Cologne, Greinstraße 6, 50939 Cologne, Germany*
[d]*Institut für Anorganische und Analytische Chemie, Universität Freiburg, Albertstraße 21, 79104 Freiburg, Germany*

†Electronic supplementary information (ESI) available: Further figures and measurements, crystallographic and electrostatic data. CSD 2081697–2081699. For ESI and crystallographic data in CIF or other electronic format see DOI: 10.1039/d1dt02189c

‡New address: School of Chemistry, University of St Andrews, North Haugh, St Andrews, Fife, KY16 9ST, UK.

(II)$_2$Sn(IV)O$_4$,[30] Fe$_4$Si$_2$Sn(II)$_6$Sn(IV)O$_{16}$[31] and in [Sn(II)$_3$Sn(IV)$_3$O$_{15}$]$^{12-}$ clusters in polyoxometalates.[32] All these structures comprise condensed Sn(II)O$_x$ (x = 3 or 4) and Sn(IV)O$_6$ polyhedra.

The stereochemically active lone pair E of Sn^{2+} acts according to Gillespie's valence-shell electron pair repulsion (VSEPR) model[33] and its extension by Andersson and Galy.[34] Accordingly, divalent tin can occur in different surroundings like distorted tetrahedra SnO$_3$E or distorted trigonal bipyramids SnO$_4$E – both are present in the structures discussed above. In contrast, tetravalent tin prefers octahedral coordination.

In this work, the crystal structures of two polymorphs of Sn(SO$_4$)$_2$ are elucidated and we report the first heterovalent tin sulfate **Sn$_2$(SO$_4$)$_3$** = Sn(II)Sn(IV)(SO$_4$)$_3$ including a careful ^{119}Sn Mössbauer spectroscopic study. The optical and thermal properties of these compounds are characterised and compared – also with the known **SnSO$_4$**.

Results and discussion

Syntheses

Crystalline **Sn$_2$(SO$_4$)$_3$** was prepared starting from SnO, B(OH)$_3$, H$_2$SO$_4$ and oleum (65% SO$_3$) *via* solvothermal synthesis in a sealed silica-glass ampoule at 180 °C. A colourless powder containing single-crystals was obtained and phase purity was confirmed by Rietveld analysis depicted in Fig. 1. The addition of B(OH)$_3$ proved to be crucial for the crystallisation under these conditions since an analogous sample without boric acid did not crystallise yielding clear solutions at synthesis temperatures of 180, 250 and 300 °C. However, after furnace treatment at 400 °C single-crystals of **Sn(SO$_4$)$_2$-I** were formed indicating a thermal conversion from **Sn$_2$(SO$_4$)$_3$** to Sn(SO$_4$)$_2$.

Single-crystals of both polymorphs **Sn(SO$_4$)$_2$-I** and **Sn(SO$_4$)$_2$-II** were obtained by solvothermal syntheses starting from metallic tin and H$_2$SO$_4$ at 400 °C. Rietveld analysis revealed a phase composition in this sample of 70% **Sn(SO$_4$)$_2$-I** and 30% **Sn(SO$_4$)$_2$-II** (Fig. S2†). Phase-pure **Sn(SO$_4$)$_2$-I** was prepared by solvothermal synthesis starting from SnO$_2$ and H$_2$SO$_4$ at 400 °C. Phase purity was confirmed by Rietveld analysis (Fig. 1). All Sn(SO$_4$)$_2$ samples were obtained in the form of pale grey powders.

Crystal structures

Sn(SO$_4$)$_2$-I: The polymorph **Sn(SO$_4$)$_2$-I** crystallises in a new structure type in space group $P2_1/c$ (no. 14) with four formula units per unit cell (Tables S4 and S5†). The unit cell is depicted in Fig. 2a, in which the sulfate tetrahedra – represented by the sulfur atoms – form a cubic closest packing with the tin atoms being situated in half of all octahedral voids. Essentially, the tin–sulfur substructure forms chains of edge-sharing SnS$_6$ octahedra and thus adopts the topology as found in the *rutile* type (Fig. 2b).

The oxygen atoms of those sulfate anions coordinate the tin ions octahedrally (Fig. S2†). Out of the four oxygen atoms of each sulfate anion only three are coordinating tin atoms with the remaining one as expected showing slightly larger atomic displacement parameters (O14 and O21) and significantly shorter S–O bonds (Table S6†). Both SO$_4$ tetrahedra can be considered regular[35] with deviations from tetrahedral symmetry of 0.37% and 0.25% calculated by the method of Balić-Žunić and Makovicky based on all ligands enclosing spheres.[36,37] The two SnO$_6$ octahedra show small deviations from the ideal symmetry of 3.08% and 2.92%. All interatomic distances are in good agreement with the sum of the respective ionic radii (Table S6†).[38]

The crystal structure of **Sn(SO$_4$)$_2$-I** was refined using data measured on a twinned specimen. This twinning is not surprising since the unit cell is close to tetragonal symmetry nicely reflecting its close relation to the *rutile* type. This unit cell coincides with the one reported by Ahmed *et al.* from indexing for the low temperature polymorph of **Sn(SO$_4$)$_2$-I**.[22]

Sn(SO$_4$)$_2$-II: It is not really surprising, that the topology of the tin–sulfur network in **Sn(SO$_4$)$_2$-II** resembles another TiO$_2$ polymorph since polymorph I was described based on rutile; polymorph II adopts an arrangement like in the high pressure phase TiO$_2$-II isotypic with the α-PbO$_2$ structure type.[39] Here, the sulfate anions form a hexagonal closest packing with tin in

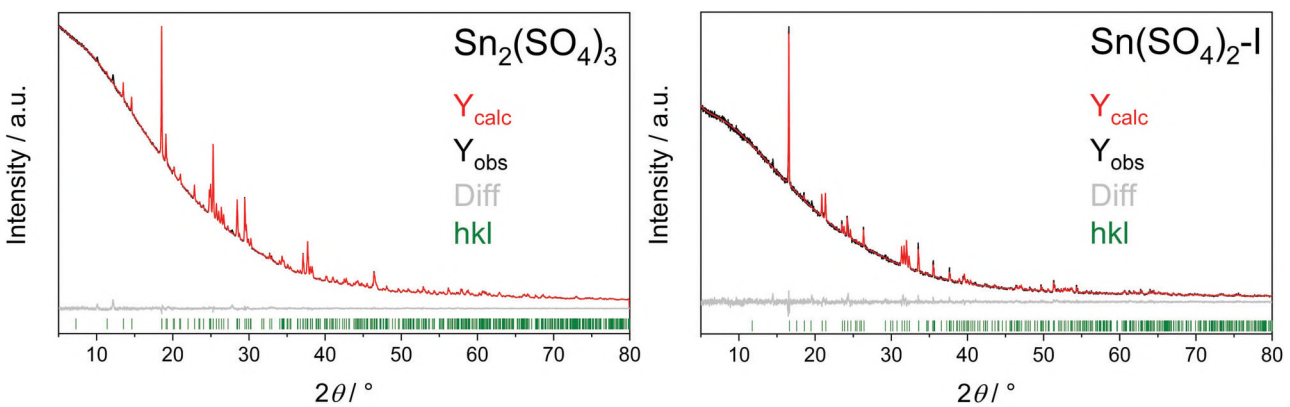

Fig. 1 Rietveld refinement of phase-pure **Sn$_2$(SO$_4$)$_3$** (left) and **Sn(SO$_4$)$_2$-I** (right); further details can be found in Tables S1–S3.†

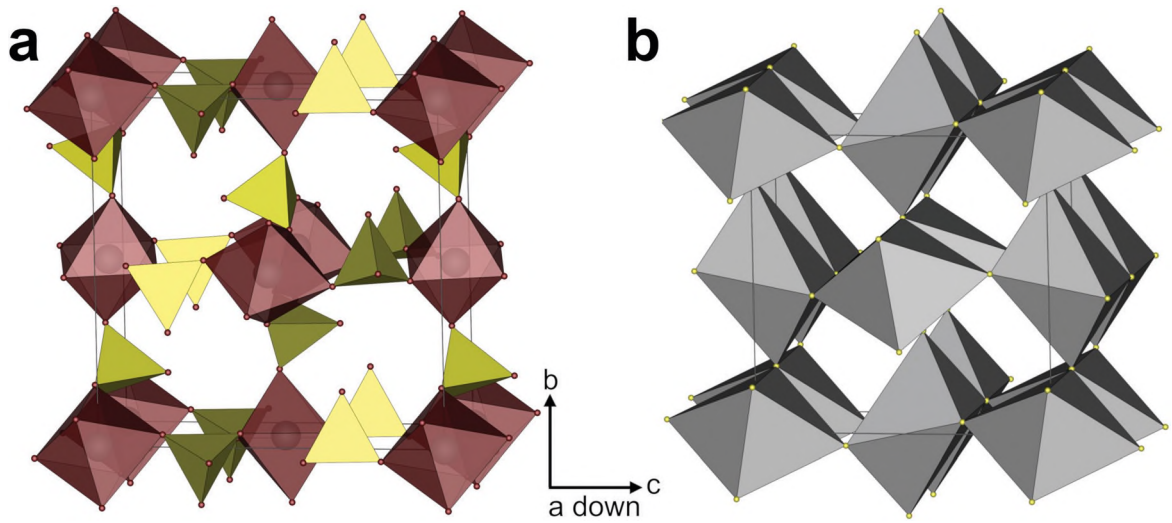

Fig. 2 (a) Unit cell of **Sn(SO$_4$)$_2$-I** viewed along (100); sulfate tetrahedra yellow, tin cations grey, oxygen atoms red, SnO_6 octahedra pale red; (b) unit cell of **Sn(SO$_4$)$_2$-I** neglecting the oxygen atoms showing the tin–sulfur substructure comprising SnS_6 octahedra in a rutile like arrangement (grey).

half of the octahedral voids. As a whole however, **Sn(SO$_4$)$_2$-II** crystallises in a new structure type in space group $P2_1/n$ (no. 14) with four formula units per unit cell (Fig. 3a, Tables S4 and S7†). Again, the oxygen atoms coordinate the tin atoms octahedrally (Fig. S3†). Analogously to **Sn(SO$_4$)$_2$-I**, each sulfate anion coordinates three cation octahedra leaving one oxygen atom per sulfate group non-coordinated. This results in one significantly shorter S–O bond (Table S8†). The impression of a denser packing of the SnO_6 and SO_4 polyhedra in **Sn(SO$_4$)$_2$-II** in comparison to **Sn(SO$_4$)$_2$-I** just by viewing both unit cells agrees with the higher density of **Sn(SO$_4$)$_2$-II**. The apparent reason can be derived comparing the underlying structure types. Rutile undergoes a first-order phase transition to the denser TiO_2-II upon pressure.[39] In both $Sn(SO_4)_2$ structures, the $Sn(SO_4)_6$ octahedra share two edges with neighbouring octahedra, in rutile-like **Sn(SO$_4$)$_2$-I** thus rods and in TiO_2-II-like **Sn(SO$_4$)$_2$-II** zig-zag chains form with the latter wriggling allowing to pack the chains denser (Fig. 3b and c). Also in **Sn(SO$_4$)$_2$-II** the two distinct SO_4 tetrahedra can be considered regular[35] with deviations from the ideal tetrahedral symmetry of 0.15% each calculated by the method of Balić-Žunić and Makovicky.[36,37] The deviation of the SnO_6 octahedron from octahedral symmetry amounts to 3.26%. Again, all interatomic distances are in good agreement with the sum of the ionic radii (Table S5†).[38]

In "The Materials Project",[40] a crystal structure for $Sn(SO_4)_2$ crystallising in an orthorhombic cell (*Pbca* (no. 61), a = 913.5 pm, b = 933.4 pm, c = 1380.5 pm, $V = 1177.07 \times 10^6$ pm^3) was deposited[41] presumably based on a calculation starting from the $Ce(SO_4)_2$ structure type and appears to be related to **Sn**

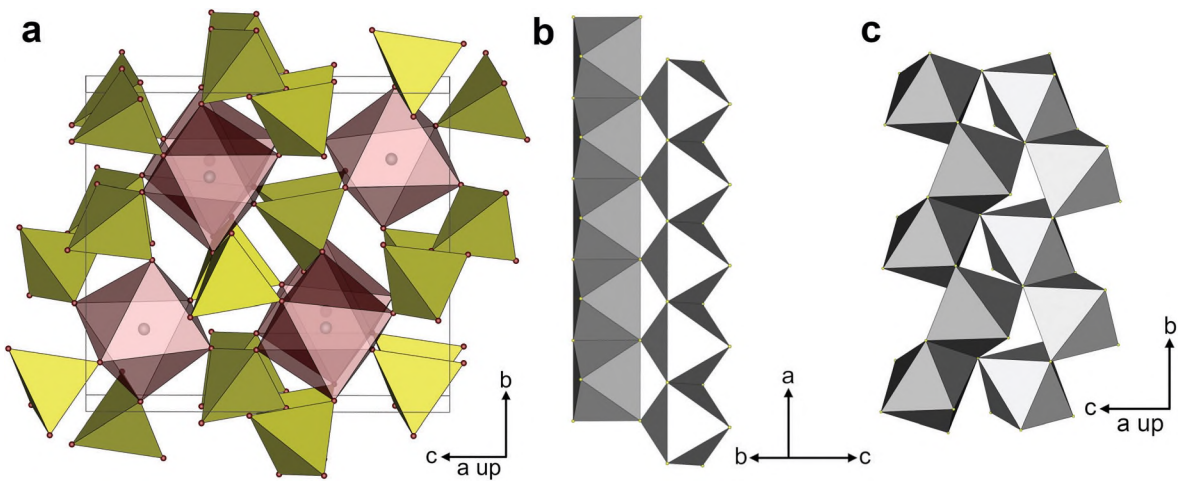

Fig. 3 (a) Unit cell of **Sn(SO$_4$)$_2$-II** viewed along (100); sulfate tetrahedra yellow, tin cations grey, oxygen atoms red, SnO_6 octahedra pale red; in (b) and (c) the SnS_6 octahedra (grey) chains *via* common edges in **Sn(SO$_4$)$_2$-I** (b) and **Sn(SO$_4$)$_2$-II** (c) are compared resembling the connection pattern of rutile and TiO_2-II, respectively; oxygen atoms are omitted for clarity.

$(SO_4)_2$-II. $P2_1/n$ is a *translationengleiche* subgroup with index 2 of *Pbca*. However, the bonding pattern in this orthorhombic form $Sn(SO_4)_2$ (*Pbca*) differs significantly from both herein described polymorphs. In these, every SnS_6 octahedron shares only two edges with neighbouring octahedra, while in this orthorhombic form this number increases to three as in *brookite*. Further comparison is prevented by the lack of information about the method used for structure determination of $Sn(SO_4)_2$ (*Pbca*).

$Sn_2(SO_4)_3$ crystallises in space group $P\bar{1}$ (no. 2) with two formula units per unit cell (Fig. 4, and Tables S4 and S9†). The cationic substructure consists of two distinct non-condensed $Sn(IV)O_6$ octahedra (Sn1 and Sn2) and $Sn(II)O_6$ non-condensed pentagonal pyramids (Sn3). These can also be viewed as distorted pentagonal bipyramidal SnO_6E in the light of the VSEPR concept (Fig. S4†). The lone pair of the Sn^{2+} cation requires space yielding respective vacant regions within the crystal structure. The anion comprises three different SO_4 tetrahedra connecting the $Sn(IV)O_6$ and $Sn(II)O_6$ polyhedra forming in a three dimensional network. The sulfate ions coordinate two Sn(IV) and two Sn(II) cations each. Consequently, there is no non-coordinating oxygen atom. Therefore, the network can be described as $(Sn(IV)O_{6/2})(Sn(II)O_{6/2})(SO_{4/2})_{12/4} \triangleq$ **$Sn_2(SO_4)_3$**.

The deviations from the ideal tetrahedral and octahedral symmetry were calculated by the method of Balić-Žunić and Makovicky based on all ligands enclosing spheres on experimental data.[36,37] The three sets of sulfate tetrahedra can be considered regular[35] with deviations of 0.05%, 0.10% and 0.11%, respectively. The $Sn(IV)O_6$ octahedra show small deviations of 2.47% and 0.96%. Selected interatomic distances and angles are tabulated in Table S10.† The distances are in good agreement with the respective sum of ionic radii.[38,42] The angles inside the $Sn(II)O_6$ pentagonal pyramid deviate from the ideal values of 90° from top to base and 72° inside the base of the pentagonal pyramid due to repulsion by the lone pair.

The crystal structure of **$Sn_2(SO_4)_3$** comprises alternating layers within the *ac* plane with exclusive Sn(IV) or Sn(II) cations, respectively. These layers are connected *via* common sulfate anions forming the **$Sn_2(SO_4)_3$** network. Consequently, the crystal structure of **$Sn_2(SO_4)_3$** can be described as a combination of alternating layers with **$SnSO_4$** and $Sn(SO_4)_2$ stoichiometry along the (010) direction. This AB stacking scheme is depicted in Fig. 5a. The $Sn(SO_4)_2$ layers comprise rutile-like rods of edge-sharing octahedra (Fig. 5b). Further, the layers are stacked in such a way that the space requirements of the stereochemically active lone pair of the Sn^{2+} cation are met (Fig. 5 and S5†). In contrast to **$SnSO_4$**, there are more oxygen atoms coordinating the Sn^{2+} cation due to the presence of adjacent layers containing $Sn(IV)O_6$ octahedra forcing the lone pair to take shape inside the layer instead of in between adjacent layers like in **$SnSO_4$**.

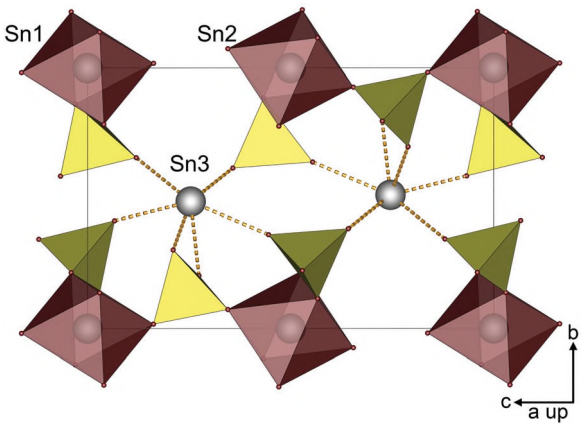

Fig. 4 Unit cell of **$Sn_2(SO_4)_3$** viewed along (100); sulfate tetrahedra yellow, tin cations grey, oxygen atoms red, SnO_6 octahedra pale red.

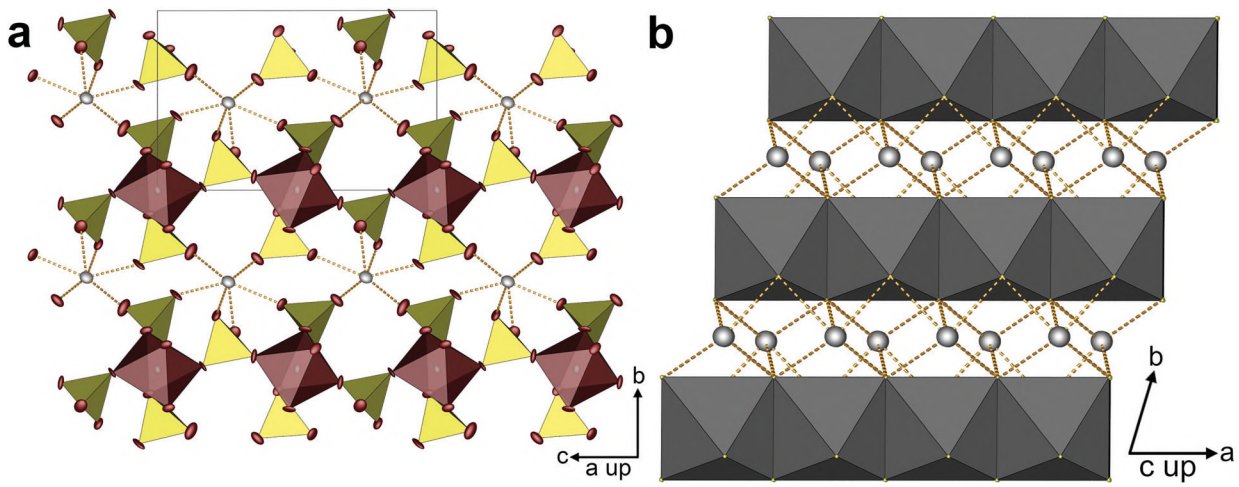

Fig. 5 Layered structure of **$Sn_2(SO_4)_3$** viewed along (100) in (a); sulfate tetrahedra yellow, tin cations grey, oxygen atoms red, SnO_6 octahedra pale red; ellipsoids are shown at 80% probability; and viewed along (001) in (b) displaying the rutile-like rods of SnS_6 octahedra (dark grey); oxygen atoms are omitted for clarity.

Consequently, $Sn_2(SO_4)_3$ is the first heterovalent tin sulfate and – to the best of our knowledge – the first compound comprising separated Sn(II)O_x (x = 6) and Sn(IV)O_6 polyhedra, *i.e.* there are no Sn(II)–O–Sn(IV) bonds. Furthermore, $Sn_2(SO_4)_3$ represents the first example for the Sn(II)O_6E distorted pentagonal bipyramidal stereochemistry. In all structures discussed in the introduction, the Sn(II)O_x (x = 3 or 4) and Sn(IV)O_6 polyhedra are condensed and the Sn^{2+} cations are fourfold coordinated at maximum.

In conclusion, all three crystal structures discussed in this contribution represent new structure types. In the case of **$Sn(SO_4)_2$-I** and **$Sn(SO_4)_2$-II**, the range of $M(SO_4)_2$ structure types is expanded beyond $Zr(SO_4)_2$ and $Ce(SO_4)_2$.[26,28] Mainly, this appears to be due to the high stability of the sixfold coordination of Sn(IV) requiring **$Sn(SO_4)_2$-I** and **$Sn(SO_4)_2$-II** to adapt a less symmetric structure than the other two structure types with coordination numbers of M of seven and eight, respectively. However, the former can be treated as related to the latter.

Electrostatic calculations

The electrostatic reasonability of the crystal structures was confirmed by calculations based on the MAPLE concept (MAdelung Part of Lattice Energy).[43] The MAPLE values for **$Sn(SO_4)_2$-I**, **$Sn(SO_4)_2$-II** and **$Sn_2(SO_4)_3$** from single-crystal data were calculated and compared to the respective sum of SnO_2, **$SnSO_4$** and SO_3 (Table S11†). The deviations are well below 1% for all structures, which is our empirical benchmark for electrostatic consistency. Moreover, all coordination numbers were confirmed by our calculations (Tables S12–14†). Especially, the calculated effective coordination numbers (Table S14†) confirm that six oxygen atoms coordinate the Sn^{2+} cation in **$Sn_2(SO_4)_3$** resulting in the distorted pentagonal bipyramidal SnO_6E discussed above.

Bond order according to Brown

The bond orders of the two modifications of $Sn(SO_4)_2$ and the mixed-valent **$Sn_2(SO_4)_3$** can be calculated following to the method of Brown.[44] According to the shorter Sn–O distances in **$Sn(SO_4)_2$-I** the sum of the bond order is higher (5.11 and 5.03) compared to **$Sn(SO_4)_2$-II** with 4.74. For the mixed-valent **$Sn_2(SO_4)_3$** the value for Sn(II) amounts to 1.54 and for Sn(IV) 5.11 and 4.98, respectively. In comparison to the values for binary tin oxides, there are significant deviations (SnO: 1.94; SnO_2 (rutile): 4.63) for **$Sn_2(SO_4)_3$** and **$Sn(SO_4)_2$-I**. Interestingly, an even higher deviation is also found for **$SnSO_4$** (1.38).

Optical properties

Infrared spectroscopy. The infrared spectra of **$Sn(SO_4)_2$-I** and **$Sn_2(SO_4)_3$** are shown in Fig. 6 in the region of 1600–400 cm^{-1} (full spectra in Fig. S6†). In accordance with reports in literature,[25,45] the observed absorptions can be attributed to various S–O vibrations. Peaking at 1377 cm^{-1} and 1344 cm^{-1} the S–O stretching vibrations of non-coordinating oxygen atoms can be found. Consequently, these bands are only present for **$Sn(SO_4)_2$-I** since in **$SnSO_4$** and **$Sn_2(SO_4)_3$** all oxygen atoms are coordinating. Further, they form a doublet due to the two distinct sets of sulfate tetrahedra in **$Sn(SO_4)_2$-I**. Below down to 800 cm^{-1} the remaining S–O stretching vibrations of coordinating oxygen atoms are located. Between 700 cm^{-1} and 400 cm^{-1} the S–O bending modes occur. At the lower end of the spectra, an overlap by Sn–O vibrations cannot be ruled out.[46] The splitting of the respective bands, *i.e.* the total number of vibrations increases from **$SnSO_4$** over **$Sn(SO_4)_2$-I** to **$Sn_2(SO_4)_3$** since the compounds comprise one, two and three distinct SO_4 groups, respectively. Further, the spectrum of **$Sn_2(SO_4)_3$** shows the discrimination between S–O stretching vibrations next to Sn(II)–O bonds above 1100 cm^{-1} and Sn(IV)–O bonds below that value. The same increase in the number of bands can be observed for the bending modes on top of the effect of the higher number of distinct SO_4 tetrahedra.

UV-vis spectroscopy. The powder reflectance spectra of **$Sn(SO_4)_2$-I** and **$Sn_2(SO_4)_3$** are shown in Fig. S7† in the range from 200 nm to 800 nm. In accordance with the colourless to pale grey powders, no absorptions in the visible region are

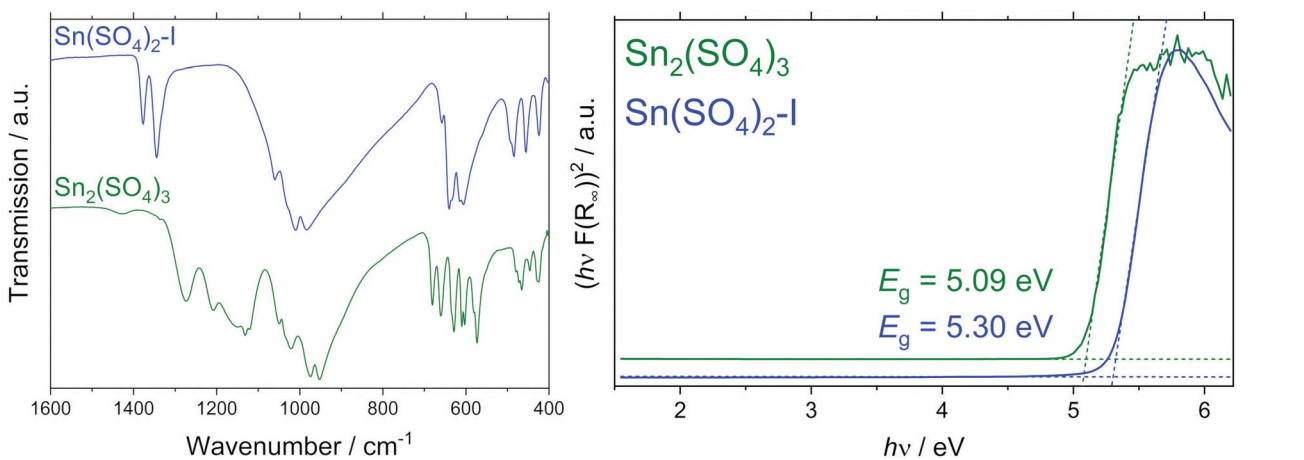

Fig. 6 Infrared spectra of **$Sn(SO_4)_2$-I** and **$Sn_2(SO_4)_3$** on the left; the full spectra can be found in Fig. S6;† Tauc-plots calculated from the UV-vis spectra of **$Sn(SO_4)_2$-I** and **$Sn_2(SO_4)_3$** on the right.

observed. For both, the fundamental absorption due to the bandgap of the samples occur in the UV regime. The bandgap energies E_g could be estimated using Tauc plots depicted in Fig. 6. The resulting E_g values are 5.30(1) eV and 5.09(1) eV for s-**Sn(SO$_4$)$_2$-I** and **Sn$_2$(SO$_4$)$_3$**, respectively. The smaller bandgap observed for **Sn$_2$(SO$_4$)$_3$** might originate from the Sn^{2+} cations. According to earlier reports,[2] **SnSO$_4$** shows an absorption in the UV region due to s–p transitions of Sn^{2+} cations at 230 nm. Such a distinct band is not observed for **Sn$_2$(SO$_4$)$_3$** despite it also containing Sn^{2+} cations.

Mössbauer spectroscopy. The experimental and simulated ^{119}Sn Mössbauer spectra (78 K data) of the **Sn(SO$_4$)$_2$-I**, **Sn$_2$(SO$_4$)$_3$** and **SnSO$_4$** samples are shown in Fig. 7. The corresponding fitting parameters are summarised in Table 1. The **Sn(SO$_4$)$_2$-I** spectrum was well reproduced with a single signal at an isomer shift of δ = −0.259 mm s^{-1}, confirming tetravalent tin. The weak quadrupole splitting parameter accounts for a deviation of the site symmetry from cubic (site symmetry $\bar{1}$). **SnSO$_4$** shows much higher quadrupole splitting as a consequence of the Sn^{II} lone pair. The divalent tin is confirmed through a large isomer shift value of δ = 3.969 mm s^{-1}. The ^{119}Sn data of our **Sn(SO$_4$)$_2$-I** and **SnSO$_4$** samples are in good agreement with literature data.[47]

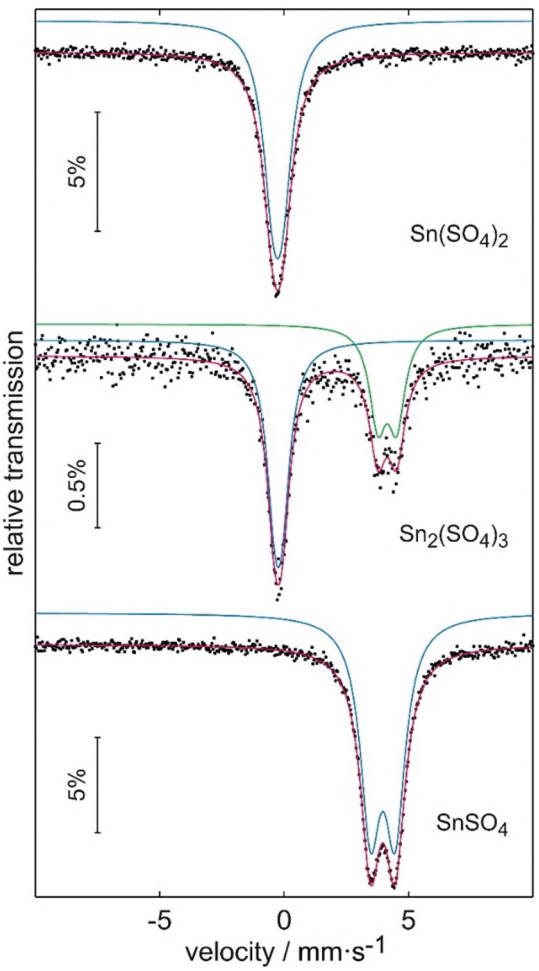

Fig. 7 Experimental (data points) and simulated (continuous line) ^{119}Sn Mössbauer spectra of **Sn(SO$_4$)$_2$-I**, **Sn$_2$(SO$_4$)$_3$** and **SnSO$_4$**. The measuring time was one day for the tin(II) and tin(IV) sulfates and five days for the mixed valence sulfate (small sample quantity).

Table 1 Fitting parameters of ^{119}Sn Mössbauer spectroscopic measurements at 78 K for the tin sulfates **Sn(SO$_4$)$_2$-I**, **Sn$_2$(SO$_4$)$_3$** and **SnSO$_4$**. δ = isomer shift, ΔE_Q = electric quadrupole splitting, Γ = experimental line width; standard deviations are given in parentheses

Compound	δ/mm s^{-1}	ΔE_Q/mm s^{-1}	Γ/mm s^{-1}	Ratio/%
Sn(IV)(SO$_4$)$_2$-I	−0.259(2)	0.376(14)	0.997(14)	100
Sn(II)Sn(IV)(SO$_4$)$_3$	−0.231(7)	0.29(4)	0.83(4)	58(2)
	4.146(14)	0.75(2)	0.82(4)	42(2)
Sn(II)SO$_4$	3.969(2)	0.992(3)	0.984(6)	100

The **Sn$_2$(SO$_4$)$_3$** sample shows two signals with a Sn(II) to Sn(IV) ratio of 58 : 42, confirming the X-ray single-crystal data. The lower signal-to-noise ratio of the **Sn$_2$(SO$_4$)$_3$** spectrum is due to the small sample quantity. Again, the Sn^{II} sub-signal shows the slightly higher quadrupole splitting parameter.

Thermal analysis

The thermal decomposition was investigated by thermogravimetric analysis (TGA) under nitrogen atmosphere and temperature programmed X-ray powder diffraction (TPXRD) inside sealed argon filled glass capillaries. The studied tin sulfates decompose according to the following reaction equations:

$$\mathbf{Sn_2(SO_4)_3} \rightarrow 2SnO_2 + 3SO_2 + O_2 \quad (1)$$

$$\mathbf{Sn(SO_4)_2} \rightarrow SnO_2 + 2SO_2 + O_2 \quad (2)$$

The expected mass losses for these processes depicted in Fig. 8 agree well with the observed values, caused by expulsion of SO_3, which in turn decomposes to SO_2 and O_2 at these temperatures. The residual powder was investigated by powder XRD confirming the formation of SnO_2 (Fig. S8†). For **Sn(SO$_4$)$_2$-I**, the temperature region of the thermal decomposition is in agreement with earlier reports.[22,24] As discussed in the introduction, Ahmed *et al.* reported high temperature polymorphism of **Sn(SO$_4$)$_2$** with a transition temperature of 500 °C.[22] Consequently, **Sn(SO$_4$)$_2$-I** was investigated by TPXRD

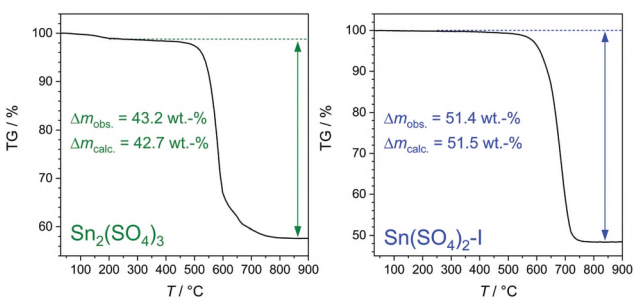

Fig. 8 Thermogravimetric analyses of **Sn$_2$(SO$_4$)$_3$** (left) and **Sn(SO$_4$)$_2$-I** (right).

confirming the decomposition towards SnO_2 above 500 °C, again. The results are shown in Fig. S9.† Moreover, the merging of some reflections is observed at 400 °C. This could indicate the existence of a tetragonal or orthorhombic high temperature polymorph. However, Rietveld analysis on this pattern starting from **$Sn(SO_4)_2$-I** from our SC-XRD structure determination was successful yielding an increased unit cell which is even closer to an orthorhombic cell than the unit cell from SC-XRD data. Details are shown in Fig. S10 and Table S3.† On the other hand, indexing on this measurement yielded an orthorhombic cell similar to the one found by Ahmed *et al.* Yet, a Pawley fit using this cell (*Pnnn* (no. 48), a = 758.97(7) pm, b = 757.47(7) pm, c = 507.68(3), R_{Bragg} = 0.004, R_{wp} = 0.049, Fig. S11†) achieved worse fitting than the Rietveld refinement with the monoclinic **$Sn(SO_4)_2$-I** structure. Possibly, this unit cell enlargement is the effect observed by Ahmed *et al.* by DTA and attributed to a phase transformation. Interestingly, equivalent **$Sn(SO_4)_2$-I** as observed at 400 °C could be prepared *via* precipitation starting from tin in H_2SO_4 as a pale grey powder without any single-crystals. The Rietveld refinement of this p-**$Sn(SO_4)_2$-I** detailed in Fig. S12 and Table S3† yielded the same enlarged unit cell as above. Further, the infrared spectra of both **$Sn(SO_4)_2$-I** samples – prepared *via* precipitation or solvothermal synthesis – displayed in Fig. S6† are almost identical confirming the results from Rietveld refinement that both compounds are indeed **$Sn(SO_4)_2$-I** with differing unit cell parameters. The TGA of the sample prepared by precipitation showed the same one step decomposition towards SnO_2. The decomposition starts at slightly lower temperatures compared to **$Sn(SO_4)_2$-I** from solvothermal synthesis (Fig. S13†). The reason for this might be the higher crystallinity of the latter sample. TPXRD performed on the **$Sn(SO_4)_2$-I** sample prepared by precipitation showed no change of the pattern before decomposition and confirmed the formation of SnO_2 (Fig. S14†). A possible explanation for the enlarged unit cell of **$Sn(SO_4)_2$-I** observed both at 400 °C and *via* the preparation by precipitation are kinetic effects. This is underlined by the PXRD pattern depicted in Fig. S15† of a **$Sn(SO_4)_2$-I** sample heated at 500 °C in inert atmosphere indicating the reversibility of the unit cell enlargement at high temperatures.

In the case of **$Sn_2(SO_4)_3$**, the reaction towards a mixture of **$SnSO_4$** and **$Sn(SO_4)_2$** is conceivable – and consistent with the TGA results since this reaction would not be accompanied by any mass loss – prior to the decomposition step towards SnO_2. However, heating a sample of **$Sn_2(SO_4)_3$** in inert atmosphere up to 450 °C, holding the temperature for 1 h and subsequent cooling yielded an unchanged PXRD (Fig. S16†). However, experiments in an open system, *i.e.* a crucible inside a muffle furnace as well as inside a sealed glass ampoule in presence of excess H_2SO_4 showed a transformation from **$Sn_2(SO_4)_3$** towards **$Sn(SO_4)_2$-I** (see Experimental section for details and Fig. S17.†) Further, the thermogravimetric data on $Sn_6O(SO_4)_9$ reported by Ahmed *et al.*[22] and our measurement on **$Sn_2(SO_4)_3$** appear to coincide. Thus, we conclude that the $Sn_6O(SO_4)_9$ prepared by Ahmed *et al.* was in reality **$Sn_2(SO_4)_3$**.

Experimental section

Syntheses

$Sn_2(SO_4)_3$: **$Sn_2(SO_4)_3$** was prepared solvothermally. 5 mmol $B(OH)_3$ (Merck, 99.5%) and 5 ml H_2SO_4 (Merck, 95–97%) were mixed inside a nitrogen flushed Schlenk flask at 200 °C for 1 h. After natural cooling to 100 °C, 0.3 ml oleum (VWR, 65% SO_3) and 1 mmol SnO (Aldrich, >99%) were added and the mixture was stirred for 1 h without further heating. Afterwards, it was transferred into a silica-glass ampoule (length 15 cm, outer diameter: 1.2 cm, wall thickness: 0.1 cm). Subsequently, the ampoule was fused and placed in a muffle furnace applying the following temperature program: heating to 180 °C with 100 K h^{-1}, holding the temperature for 60 h, and cooling down to room temperature with 100 K h^{-1}. The ampoule was opened after cooling with liquid nitrogen (*Caution*! During and even after the reaction the ampoules are under remarkable pressure and must therefore be handled with great care). After decantation of the excess sulfuric acid, the sample was washed with 5 ml anhydrous acetonitrile (Acros, 99.9%, extra dry) using a frit in a Schlenk line under N_2 atmosphere. Afterwards, the product was stored in a compartment dryer for 24 h at 180 °C and subsequently transferred to an argon filled glovebox. With the exception **$SnSO_4$**, all products are sensitive towards moisture and hence were stored under inert conditions for further investigations.

Synthesis without the addition of $B(OH)_3$ yielded no crystallisation at synthesis temperatures of 180 °C, 250 °C and 300 °C (temperature hold for 60 h each time). However, after furnace treatment at 400 °C phase-pure **$Sn(SO_4)_2$-I** was obtained.

$Sn(SO_4)_2$: A mixture of **$Sn(SO_4)_2$-I** and **$Sn(SO_4)_2$-II** containing the single-crystals used for structure determination was prepared *via* solvothermal synthesis. 3.2 mmol tin (Alfa Aesar, >99.5%) was mixed with 3.4 ml H_2SO_4 inside a nitrogen flushed Schlenk flask at 200 °C and stirred for 1 h before transfer into a silica-glass ampoule. The ampoule was fused, placed in a muffle furnace and heated to 400 °C for 24 h (heating and cooling ramps 100 K h^{-1}). The ampoule was opened after cooling with liquid nitrogen and – after decantation of excess sulfuric acid – placed inside a muffle furnace preheated to 150 °C and heated at 300 °C for 60 h. Afterwards, the dry product was taken out of the furnace at a temperature of 150 °C and transferred to an argon filled glovebox.

Phase-pure **$Sn(SO_4)_2$-I** was prepared *via* solvothermal synthesis mixing 1.6 mmol SnO_2 and 1.7 ml H_2SO_4 inside a nitrogen flushed Schlenk flask at 200 °C under constant stirring for 1 h before transfer into a silica-glass ampoule. Subsequently, the same steps were applied as for the mixed sample detailed above.

Alternatively, **$Sn(SO_4)_2$-I** was prepared *via* precipitation. Therefore, 3.2 mmol tin were mixed with 5 ml H_2SO_4 inside a nitrogen flushed Schlenk flask and stirred at 300 °C for 1 h. The resulting precipitate was washed with 5 ml anhydrous acetonitrile using a frit in a Schlenk line under N_2 atmosphere. Afterwards, the product was transferred to an argon filled glovebox. The relationship of the **$Sn(SO_4)_2$-I** samples prepared by

precipitation and solvothermal synthesis is detailed in the thermal analysis chapter.

$SnSO_4$: $SnSO_4$ was synthesised *via* room temperature precipitation of 2.33 mmol $SnCl_2{\cdot}2H_2O$ (Merck, >96%) in 5 ml H_2SO_4 inside a nitrogen flushed Schlenk flask under constant stirring. The precipitate was washed with 5 ml anhydrous acetonitrile using a frit in a Schlenk line under N_2 atmosphere. **$SnSO_4$** was obtained as a colourless and phase-pure powder (Fig. S18†).

Single-crystal structure determination

Immediately after opening the ampoule, single-crystals were transferred into perfluorinated polyether. Suited single-crystals of **$Sn(SO_4)_2$-I**, **$Sn(SO_4)_2$-II** and **$Sn_2(SO_4)_3$** were selected for single-crystal X-ray diffraction (XRD) under a polarised light microscope. Diffraction data was collected with a Bruker D8 Venture diffractometer using Mo-K_α radiation (λ = 0.7093 Å). Absorption correction was performed by the multiscan method. The structures were solved by Direct Methods and refined by full-matrix least-squares technique with the SHELXTL crystallographic software package.[48] **$Sn(SO_4)_2$-I** was refined as a two domain twin. Relevant crystallographic data and further details of the structure determinations are summarised in Tables S4–S10.†

Further details of the crystal structure investigations may be obtained at https://www.ccdc.cam.ac.uk/ on quoting the depository numbers CSD 2081698 (**$Sn(SO_4)_2$-I**), 2081699 (**$Sn(SO_4)_2$-II**), 2081697 (**$Sn_2(SO_4)_3$**),† the names of the authors, and citation of this publication.

Powder X-ray diffraction (PXRD)

The samples were ground and filled into a Hilgenberg glass capillary (outer diameter 0.3 mm, wall thickness 0.01 mm) inside an argon filled glovebox. The data was collected with a Bruker D8 Advance diffractometer with Cu-K_α radiation (λ = 1.54184 Å) with a 1D LynxEye detector, steps of 0.02° and transmission geometry. The generator was driven at 40 kV and 40 mA. The background at lower diffraction angles is due to the absorption of the glass capillary.

Temperature-programmed Powder X-ray Diffraction (TPXRD) was performed with the same device using a furnace attachment and a silica-glass Hilgenberg capillary (outer diameter 0.3 mm, wall thickness 0.01 mm). The strong background between 12.5° < 2θ < 30° is due to the used furnace attachment.

The non-hygroscopic powders, *e.g.* the thermal decomposition products (for further details see Thermal analysis) or **$SnSO_4$** were measured with a Seifert 3003 TT diffractometer at room temperature in Bragg–Brentano geometry using Cu-K_α radiation (λ = 1.54184 Å), a GE METEOR 1D line detector and a Ni-Filter to suppress K_β radiation (X-ray tube operated at 40 kV and 40 mA, scan range: 5–80°, increment: 0.02°, 40 scans per data point, integration time: 200 s per degree, variable divergence slit).

Rietveld refinement

Analysis of diffraction data was performed using the Rietveld method with the program TOPAS V.[49] The instrumental resolution function was determined empirically from a set of fundamental parameters using a reference scan of Si (NIST 640d).[50] The structural models of **$Sn(SO_4)_2$-I**, **$Sn(SO_4)_2$-II** and **$Sn_2(SO_4)_3$** from our single-crystal XRD measurement were used as starting models for Rietveld analysis. The isotropic displacement parameters were constrained to one common value for each atom type (Sn, S and O). For **$Sn_2(SO_4)_3$**, they were fixed to the values determined by single-crystal XRD in order to minimise quantification errors. Details are displayed in Tables S1–S3, and Fig. 1 and S1.†

FTIR spectroscopy

The Fourier-transform infrared spectra were recorded at room temperature with a Bruker EQUINOX 55 T-R spectrometer using a Platinum ATR device (scan range: 400–4000 cm^{-1}, resolution: 2 cm^{-1}, 32 scans per sample).

UV-vis spectroscopy

The UV-vis spectra were recorded as diffuse reflection spectra at room temperature with a Varian Cary 300 Scan UV-vis spectrophotometer using an Ulbricht sphere detector and a deuterium lamp/mercury lamp light source (scan range: 200–800 nm, increment 1 nm, scan rate: 120 nm min^{-1}).

^{119}Sn Mössbauer spectroscopy

A $Ca^{119m}SnO_3$ source was used for the Mössbauer spectroscopic experiments on the **$Sn(SO_4)_2$-I**, **$Sn_2(SO_4)_3$** and **$SnSO_4$** samples. The measurements were carried out in a standard liquid nitrogen bath cryostat at 78 K. The Mössbauer source was kept at room temperature. The samples were enclosed in small PMMA containers at an optimised thickness.[51] Fitting of the data was done by using the WinNormos for Igor6 program package.[52]

Thermal analysis

The thermogravimetric analyses (TGA) were performed with a NETZSCH STA 409 PC Luxx thermobalance under N_2 atmosphere with 70 mL min^{-1} flow in alumina crucibles (heating rate: 10 K min^{-1}). The residues after these measurements were investigated by powder diffraction.

Additionally, as-prepared **$Sn_2(SO_4)_3$** was heat treated inside the TGA instrument for 1 h at 450 °C in order to investigate its thermal decomposition intermediates. Another sample was heated at 300 °C inside a muffle furnace at air for 24 h. Further, as-prepared **$Sn(SO_4)_2$-I** was heat treated inside the TGA instrument for 1 h at 500 °C. All samples were investigated by PXRD after heat treatment.

Conclusions

In this work, the crystal structures of **$Sn(SO_4)_2$-I**, **$Sn(SO_4)_2$-II** and **$Sn_2(SO_4)_3$** are elucidated for the first time representing three new structure types. The latter is the first heterovalent pure tin sulfate and the first compound comprising non-condensed $Sn(II)O_6$ and $Sn(IV)O_6$ polyhedra. Further, it comprises

alternating layers with $\mathbf{Sn(SO_4)_2}$ and $\mathbf{SnSO_4}$ stoichiometry. Interestingly, the two polymorphs can be traced back to simple structure types as rutile ($\mathbf{Sn(SO_4)_2}$-**I**) and TiO_2-II/α-PbO_2 ($\mathbf{Sn(SO_4)_2}$-**II**).

The optical and thermal properties of these tin sulfates were investigated and compared to $\mathbf{SnSO_4}$ – the only tin sulfate with already known crystal structure. Infrared and ^{119}Sn Mössbauer spectroscopy could confirm the structure determination by the single-crystal XRD in the sense of the various connection pattern and oxidation states of tin, respectively. The band gaps of the compounds could be estimated by UV-vis spectroscopy. Moreover, the thermal decomposition process towards SnO_2 was explored in detail including possible conversion pathways from one tin sulfate to another. Thus, $\mathbf{Sn_2(SO_4)_3}$ can be converted to $\mathbf{Sn(SO_4)_2}$-**I** in oxidising conditions.

Consequently, we could enrich the ternary main group element system Sn–S–O significantly, which might trigger future research. With respect to NLO materials, the introduction of halogen ions might foster non-centrosymmetric structures as observed in tin borate fluorides[7] or sulfate fluorides or chlorides.[4,5]

Author contributions

M. H. conducted all experiments and analyses not noted otherwise, solved the crystal structure of $\mathbf{Sn_2(SO_4)_3}$, prepared all visualisation and wrote the original draft. P. N. conducted the solvothermal syntheses of $Sn(SO_4)_2$, solved the crystal structures of $\mathbf{Sn(SO_4)_2}$-**I** and $\mathbf{Sn(SO_4)_2}$-**II**, and did an initial characterisation of $Sn(SO_4)_2$. M. D. also conducted solvothermal syntheses of $Sn(SO_4)_2$, independently solved the crystal structures of $\mathbf{Sn(SO_4)_2}$-**I** and $\mathbf{Sn(SO_4)_2}$-**II** under supervision of H. H.; S. K. performed the ^{119}Sn Mössbauer spectroscopic measurements under supervision of R. P.; K. N. and M. S. prepared $\mathbf{Sn(SO_4)_2}$-**I** and solved its crystal structure independently under the supervision of M. W.; H. A. H. supervised all the work. All authors reviewed and edited the final draft of the manuscript.

Conflicts of interest

There are no conflicts to declare.

Acknowledgements

H. A. H. and P. N. thank the Deutsche Forschungsgemeinschaft (DFG) for financial support under the project HO 4503/5-1.

References

1 X. Zhang, W. Jiang, Q. Pan, G. Yuan and H. J. Seo, *Mater. Lett.*, 2014, **128**, 89–92.
2 H. Donker, W. M. A. Smit and G. Blasse, *Phys. Status Solidi B*, 1988, **148**, 413–419.
3 R. Cong, Y. Wang, L. Kang, Z. Zhou, Z. Lin and T. Yang, *Inorg. Chem. Front.*, 2015, **2**, 170–176.
4 K. Chen, Y. Yang, G. Peng, S. Yang, T. Yan, H. Fan, Z. Lin and N. Ye, *J. Mater. Chem. C*, 2019, **7**, 9900–9907.
5 X. Dong, L. Huang, C. Hu, H. Zeng, Z. Lin, X. Wang, K. M. Ok and G. Zou, *Angew. Chem., Int. Ed.*, 2019, **58**, 6528–6534.
6 (*a*) S. G. Jantz, M. Dialer, L. Bayarjargal, B. Winkler, L. van Wüllen, F. Pielnhofer, J. Brgoch, R. Weihrich and H. A. Höppe, *Adv. Opt. Mater.*, 2018, **7**, 1800497; (*b*) M. Luo, F. Liang, Y. Song, D. Zhao, N. Ye and Z. Lin, *J. Am. Chem. Soc.*, 2018, **140**, 6814–6817.
7 S. Schönegger, S. G. Jantz, A. Saxer, L. Bayarjargal, B. Winkler, F. Pielnhofer, H. A. Höppe and H. Huppertz, *Chem. – Eur. J.*, 2018, **24**, 16036–16043.
8 S. M. Haile, D. A. Boysen, C. R. Chisholm and R. B. Merle, *Nature*, 2001, **410**, 910–913.
9 C. Cascales, B. G. Lor, E. G. Puebla, M. Iglesias, M. A. Monge, C. R. Valero and N. Snejko, *Chem. Mater.*, 2004, **16**, 4144–4149.
10 (*a*) Y. Li, F. Liang, S. Zhao, L. Li, Z. Wu, Q. Ding, S. Liu, Z. Lin, M. Hong and J. Luo, *J. Am. Chem. Soc.*, 2019, **141**, 3833–3837; (*b*) P. Netzsch, H. Bariss, L. Bayarjargal and H. A. Höppe, *Dalton Trans.*, 2019, **48**, 16377–16383; (*c*) A. Lakshmanan, S.-B. Kim, B. G. Kum, H. M. Jang and B. K. Kang, *Phys. Status Solidi A*, 2006, **203**, 565–577; (*d*) H. A. Höppe, *Angew. Chem., Int. Ed.*, 2009, **48**, 3572–3582.
11 M. Hämmer, L. Bayarjargal and H. A. Höppe, *Angew. Chem.*, 2021, **60**, 1503–1506.
12 A. Magnusson and L.-G. Johansson, *Acta Chem. Scand.*, 1982, **36a**, 429–433.
13 G. Lundren, G. Wernfors and T. Yamaguchi, *Acta Crystallogr., Sect. B: Struct. Crystallogr. Cryst. Chem.*, 1982, **38**, 2357–2361.
14 J. D. Donaldson and D. C. Puxley, *Acta Crystallogr., Sect. B: Struct. Crystallogr. Cryst. Chem.*, 1972, **28**, 864–867.
15 S. M. Antao, *Powder Diffr.*, 2012, **27**, 179–183.
16 F. C. Mathers and H. S. Rothrock, *Ind. Eng. Chem.*, 1931, **23**, 831–832.
17 (*a*) S. Grimvall, S. Husebye, Å. Rolandsen, A. F. Andresen and P. Fischer, *Acta Chem. Scand.*, 1975, **29a**, 590–598; (*b*) C. G. Davies, J. D. Donaldson, D. R. Laughlin, R. A. Howie and R. Beddoes, *J. Chem. Soc., Dalton Trans.*, 1975, 2241.
18 A. J. Locock, R. A. Ramik and M. E. Back, *Can. Mineral.*, 2006, **44**, 1457–1467.
19 S. Grimvall, *Acta Chem. Scand.*, 1982, **36a**, 361–364.
20 I. V. Pekov, E. V. Sereda, N. V. Zubkova, V. O. Yapaskurt, N. V. Chukanov, S. N. Britvin, I. S. Lykova and D. Y. Pushcharovsky, *Eur. J. Mineral.*, 2018, **30**, 375–382.
21 (*a*) C. Logemann, J. Witt, D. Gunzelmann, J. Senker and M. S. Wickleder, *Z. Anorg. Allg. Chem.*, 2012, **638**, 2053–2061; (*b*) C. Logemann, D. Gunzelmann, T. Klüner,

J. Senker and M. S. Wickleder, *Chem. – Eur. J.*, 2012, **18**, 15495–15503.
22 M. A. K. Ahmed, H. Fjellvåg, A. Kjekshus, L. V. Vilkov, R. Sillanpää, G. Bernáth, J. Szúnyog and B. Långström, *Acta Chem. Scand.*, 1998, **52**, 305–311.
23 (*a*) M. S. Wickleder and C. Logemann, in *Handbook of Chalcogen Chemistry: New Perspectives in Sulfur, Selenium and Tellurium (2)*, The Royal Society of Chemistry, 2013, vol. 1, pp. 307–345; (*b*) R. C. Ropp, *Encyclopedia of the alkaline earth compounds*, Elsevier, Oxford, 2013; (*c*) E. G. Rochow and E. W. Abel, *The Chemistry of Germanium. Tin and Lead*, Pergamon Press, Oxford, 1973, vol. 14; (*d*) G. Brauer, *Handbuch der Präparativen Anorganischen Chemie*, Ferdinand Enke Verlag, Stuttgart, 1975–1981; (*e*) C. H. Brubaker, *J. Am. Chem. Soc.*, 1954, **76**, 4269–4271.
24 K. H. Stern, *High temperature properties and thermal decomposition of inorganic salts with oxyanions*, CRC Press, Boca Raton, Fla, 2001.
25 I. J. Dijs, R. de Koning, J. W. Geus and L. W. Jenneskens, *Phys. Chem. Chem. Phys.*, 2001, **3**, 4423–4429.
26 I. J. Bear and W. G. Mumme, *Acta Crystallogr., Sect. B: Struct. Crystallogr. Cryst. Chem.*, 1970, **26**, 1140–1145.
27 U. Betke and M. S. Wickleder, *Eur. J. Inorg. Chem.*, 2012, **2012**, 306–317.
28 D. L. Rogachev, M. A. Porai-Koshits, V. Y. Kuznetsov and L. M. Dikareva, *J. Struct. Chem.*, 1974, **15**, 397–401.
29 D. J. Stewart, O. Knop, R. E. Meads and W. G. Parker, *Can. J. Chem.*, 1973, **51**, 1041–1049.
30 T. A. White, M. S. Moreno and P. A. Midgley, *Z. Kristallogr.*, 2010, **225**, 274.
31 T. Söhnel, P. Böttcher, W. Reichelt and F. E. Wagner, *Z. Anorg. Allg. Chem.*, 1998, **624**, 708–714.
32 K. Suzuki, T. Hanaya, R. Sato, T. Minato, K. Yamaguchi and N. Mizuno, *Chem. Commun.*, 2016, **52**, 10688–10691.
33 (*a*) R. J. Gillespie, *J. Chem. Soc.*, 1963, 4672; (*b*) R. J. Gillespie, *J. Chem. Educ.*, 1963, **40**, 295; (*c*) R. J. Gillespie, *Coord. Chem. Rev.*, 2008, **252**, 1315–1327.
34 (*a*) S. Andersson, A. Åström, J. Galy and G. Meunier, *J. Solid State Chem.*, 1973, **6**, 187–190; (*b*) J. Galy, G. Meunier, S. Andersson and A. Åström, *J. Solid State Chem.*, 1975, **13**, 142–159.
35 H. A. Höppe, *J. Solid State Chem.*, 2009, **182**, 1786–1791.
36 T. Balić Žunić and E. Makovicky, *Acta Crystallogr., Sect. B: Struct. Sci.*, 1996, **52**, 78–81.
37 E. Makovicky and T. Balić-Žunić, *Acta Crystallogr., Sect. B: Struct. Sci.*, 1998, **54**, 766–773.
38 R. D. Shannon, *Acta Crystallogr., Sect. A: Cryst. Phys., Diffr., Theor. Gen. Crystallogr.*, 1976, **32**, 751–767.
39 S. K. Filatov, N. A. Bendeliani, B. Albert, J. Kopf, T. I. Dyuzheva and L. M. Lityagina, *Dokl. Phys.*, 2007, **52**, 195–199.
40 A. Jain, S. P. Ong, G. Hautier, W. Chen, W. D. Richards, S. Dacek, S. Cholia, D. Gunter, D. Skinner, G. Ceder and K. A. Persson, *APL Mater.*, 2013, **1**, 11002.
41 K. Persson, *Materials Data on $Sn(SO_y)_2$ (SG:61) by Materials Project*, 2016, DOI: 10.17188/1291365.
42 A. A. B. Baloch, S. M. Alqahtani, F. Mumtaz, A. H. Muqaibel, S. N. Rashkeev and F. H. Alharbi, *Phys. Rev. Mater.*, 2021, **5**, 1080.
43 (*a*) R. Hübenthal, *MAPLE. Program for the Calculation of the Madelung Part of Lattice Energy*, Universität Gießen, Gießen, 1993; (*b*) R. Hoppe, *Angew. Chem.*, 1966, **78**, 52–63; (*c*) R. Hoppe, *Angew. Chem., Int. Ed. Engl.*, 1970, **9**, 25–34; (*d*) R. Hoppe, *Z. Kristallogr.*, 1979, **150**, 23–52.
44 I. D. Brown, *The Chemical Bond in Inorganic Chemistry*, Oxford Univ. Press, 2009.
45 (*a*) E. E. Platero and M. P. Mentruit, *Catal. Lett.*, 1995, **30**, 31–39; (*b*) J. Weidlein, U. Müller and K. Dehnicke, *Schwingungsfrequenzen*, Thieme, Stuttgart, 1981.
46 R. S. Katiyar, P. Dawson, M. M. Hargreave and G. R. Wilkinson, *J. Phys. C: Solid State Phys.*, 1971, **4**, 2421–2431.
47 J. K. Lees and P. A. Flinn, *J. Chem. Phys.*, 1968, **48**, 882–889.
48 G. M. Sheldrick, *Acta Crystallogr., Sect. C: Struct. Chem.*, 2015, **71**, 3–8.
49 Bruker AXS, *Topas V5, General profile and structure analysis software for powder diffraction data. User's Manual*, Karlsruhe, Germany, 2014.
50 R. W. Cheary, A. A. Coelho and J. P. Cline, *J. Res. Natl. Inst. Stand. Technol.*, 2004, **109**, 1–25.
51 G. J. Long, T. E. Cranshaw and G. Longworth, *Moessbauer Eff. Ref. Data J.*, 1983, **6**, 42–49.
52 R. A. Brand, *WINNORMOS for IGOR6, version for IGOR6.2 or above: 22/02/2017*, Universität Duisburg, Duisburg, Germany, 2017.